

Optimization of Standalone Microgrid Considering Active Damping Technique and Smart Power Management using Fuzzy Logic Supervisor

Fadoul Souleyman Tidjani, *Student Member IEEE*, Abdelhamid Hamadi, *Member IEEE*, Ambrish Chandra, *Fellow, IEEE*, Pragassen Pillay, *Fellow, IEEE* and Auguste Ndtoungou

Abstract— Microgrid (MG) is attracting considerable attention as a solution to energy deficiency, especially, in remote areas. A microgrid (MG) is defined as a group of interconnected loads and multiple distributed generators that are usually integrated via voltage source convertors (VSC) and is able to operate in both grid-connected or island-mode. In order to enhance power quality and power energy management reliability, MG needs optimization in terms of control and size reduction of components. To make some contributions, this paper analyzes three aspects: 1) Developing a new approach of active damping technique based on mathematical model of voltage source convertor without any additional sensors; 2) Reducing the size of the output LC filter by shifting the frequency and adjusting the active damping coefficient; 3) Building a strong fuzzy logic supervisor for smart power management. The simulation and experimental results demonstrate excellent performance of the proposed design and control approaches.

Index Terms— Microgrid (MG); Photovoltaic Array (PVA); Voltage Source Converter (VSC); Active Damping Control (ADC); Fuzzy Logic Supervisor (FLS)

I. INTRODUCTION

In many countries of the world, it is usually difficult to extend the power grid to remote areas due to a variety of reasons including economic factors and reliability issues. As a result, many communities use independent diesel generators or firewood for daily energy needs. Because of cost of the fuel and its transportation, the capacity of power supplies on those remote areas are very limited and has a negative impact on the economic development of those regions [1]. However, many remote areas are normally rich in renewable energy that could be a key factor to solve the power supply problems when used adequately. Over the past years, different concepts of microgrid (MG) have been proposed by academicians and industry professionals in order to solve the power supply problems in remote areas [2]-[7]. The MG system is generally based on renewable energy sources (RES) such as wind, solar, and hydro, but these type of energies are usually stochastic and intermittent [8]. So, it is essential to make effective use of RES while keeping a stable, reliable, and economic operation of MG. Much research has been made to pursue the optimization of MG system. One of the focuses is the optimal sizing of voltage source converter (VSC) which is generally considered in MG as a main key for a robust operation [9]. A special attention has been paid on multiple parameters such as sizing of the VSC output filter, the battery protection and the smart power management. In [10]-[11], a design procedure of a shunt RC damper has been proposed for the LCL filter to allow deriving useful expressions for the actual resonance frequency of the filter, quality factor, and the damping resistor that ensures that the peak in the filter admittance is minimal.

However, the presence of the damping resistance always leads to power loss and less attenuation around the switching frequency. To overcome these drawbacks, the active damping control (ADC) have been proposed in [12]-[14], with the basic idea of replacing the physical damping resistor through modifying the converter control algorithm. On the other hand, this modification requires usually one or more additional filter variables and sensors, so this may increase the complexity of the system control which could make it less reliable. In addition, the VSC parameters optimization is not the only parameters to ensure a high reliability of the system. Therefore, the MG requires a smart power management adapting to the real case in order to optimize the system operation. Diverse algorithms based on fuzzy logic, nonlinear control, predictive and adaptive control [15]-[28] are proven to be effective in smart power management for various applications.

Major contributions of this paper are listed as follows. 1) Developing a new approach of the active damping by introducing a new k_c^*ic expression on dynamical voltage and modify capacitor current in the VSC mathematical model. This approach allows reducing the damping resonance and increasing the attenuation which helps for better filtering of high voltage frequency of the VSC, 2) the second contribution is the size reduction of the output LC filter by shifting the resonance frequency and 3) the third contribution is focused on smart power management using fuzzy logic supervisor. This paper is organized as follows. Section II describes the system and Section III explains the VSC mathematical model and control algorithm. Section IV describes the proposed mathematical model of active damping technique and the output filter optimization. Section V explains the strategy of fuzzy logic supervisor rules to manage the power flow of the system. In Section VI, the simulation and experimental results are discussed and finally, the section VII concludes the paper.

II. SYSTEM DESCRIPTION AND SIZING

A. System description

The system under study as shown in Fig.1 is a standalone microgrid for remote area in republic of Chad. It consists of PVA, VSC, Gas generator Set, dc water pump as a damping load and electric vehicle. The total peak power is 37 kW based on the critical scenario when the PVA does not generate any power and the load demand is the maximum.

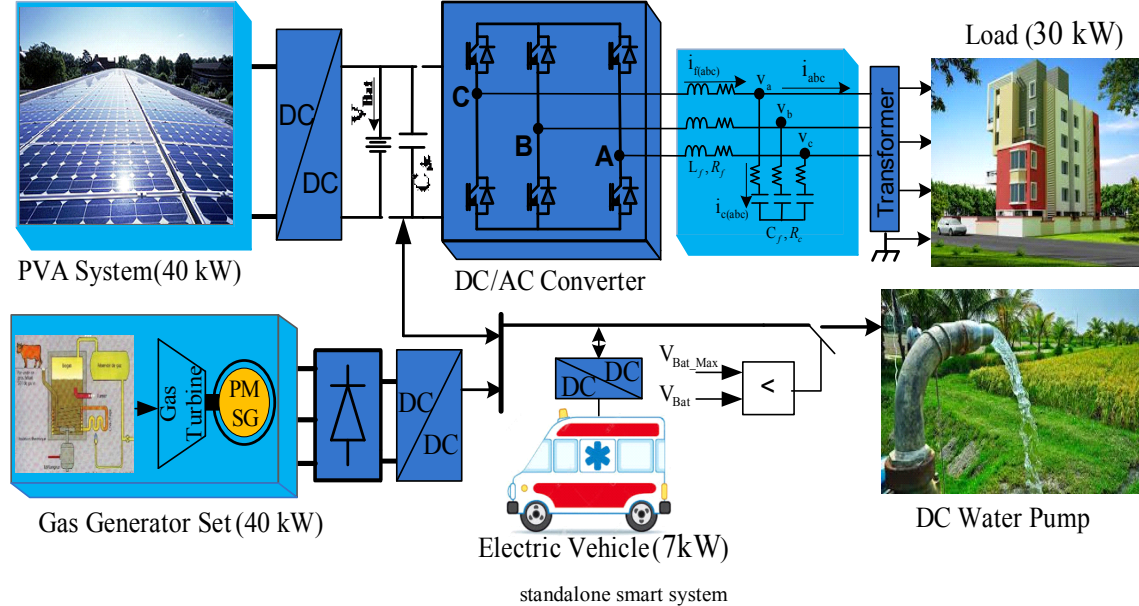


Fig. 1. Hybrid

B. Calculation of the PVA size

Step1: Estimation of the daily energy consumption

The total peak power is $P_{\text{total}} = 37 \text{ kW}$ as shown in Fig.2. The daily energy consumption is calculated using the solar radiation data of the region (Fig.3)

$$E_{\text{daily}} = P_{\text{total}} * T = 37 * 6.9 = 255 \text{ kWh} \quad (1)$$

Where T is the peak sunlight hour equivalent to the number of hours per day when the average solar irradiance is 1000 W/m^2 . From Fig.3, lets us choose $T=6.9 \text{ hr}$ that represents the worst scenario where the solar irradiation is the minimum.

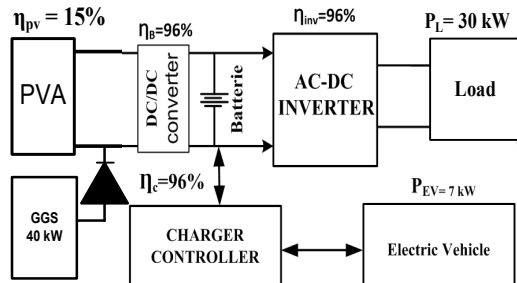


Fig 2 Peak power estimation

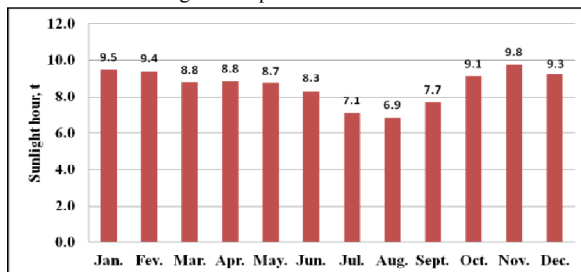


Fig 3 Average daily sunlight hour in the Sahelian Zone of Africa

Step2: Calculation of the PVA size

For this calculation, the photovoltaic module “SER-220P-WHT” of “SunPower Inc” is used. The technical data per unit is given by:

$$P_{\text{PVmodule}} = 220 \text{ W}, V_{\text{mpp}} = 29.4 \text{ V}, \text{area } S_{\text{PV}} = 1.64 \text{ m}^2.$$

The maximum PVA size is then calculated as:

$$P_{\text{PVAmax}} = \frac{P_L}{\eta_B \cdot \eta_{\text{inv}}} + \frac{P_{\text{EV}}}{\eta_B \cdot \eta_c} = \frac{30 + 7}{0.96 * 0.96} = 40 \text{ kW} \quad (2)$$

Where η_B , η_c and η_{inv} are the efficiency of dc-dc converter, EV battery charger and the inverter respectively.

The total number of PV modules to be installed is $N_T = N_P \cdot N_S$ where the number of PV modules to be installed in parallel $N_P = \frac{P_{\text{PVAmax}}}{P_{\text{PVmodule}} \cdot N_s} = \frac{40000}{220 \cdot 8} = 23$ the number of PV modules to be installed in series $N_s = \frac{\text{voltage of use}}{\text{voltage of module}} = \frac{220}{29.4} = 8$. So $N_T = N_s \cdot N_P = 184$ and the corresponding area of the PVA is: $S_{\text{PVA}} = S_{\text{PVmodule}} \cdot N_T = 1.64 \cdot 184 = 302 \text{ m}^2$.

C. Calculation of the battery size:

The battery size is chosen to be used only for emergency or for a few times during the start-up of the Gas generator when the PVA does not generate any power. The total battery capacity in ampere-hour for 2 hours autonomy is calculated as following:

$$C_{\text{total}} = \frac{E_{\text{battery}}}{V_{\text{bat}}} = \frac{74000}{500} \approx 148 \text{ Ah} \quad (3)$$

with $E_{\text{battery}} = P_t \cdot t = 37 \text{ kW} \cdot 2 \text{ hr} = 74 \text{ kWhr}$

D. Maximum power tracking of the PVA

The diagram of perturb and observe algorithm used to track the maximum available power from photovoltaic is shown in fig.4.

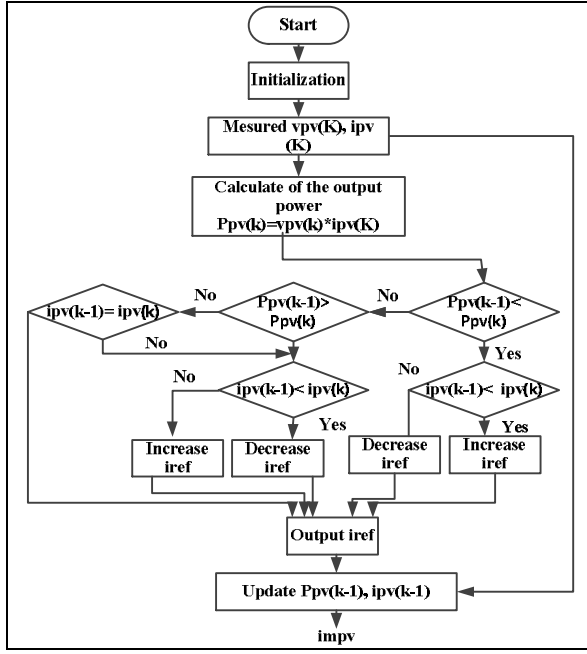


Fig.4 Perturb and observe technique for MPPT

III. VOLTAGE SOURCE CONVERTOR CONTROL MODEL

The voltage equations of DC/AC converter and its control law are given by [29]-[30]:

$$\begin{aligned} L_f \frac{di_{fa}}{dt} + R_f i_{fa} &= u_1 - v_a \\ L_f \frac{di_{fb}}{dt} + R_f i_{fb} &= u_2 - v_b \\ L_f \frac{di_{fc}}{dt} + R_f i_{fc} &= u_3 - v_c \end{aligned} \quad (4)$$

where u_1 , u_2 and u_3 are the control laws; v_a , v_b and v_c the load voltage; i_{fa} , i_{fb} , and i_{fc} the filter currents.

Integrating the regulation of the PI controller, the following equations are derived.

$$\begin{aligned} \underbrace{L_f \frac{di_{fa}}{dt} + R_f i_{fa}}_{u_{fa}} &= u_1 - v_a \rightarrow u_1 = v_a + u_{fa} \\ \underbrace{L_f \frac{di_{fb}}{dt} + R_f i_{fb}}_{u_{fb}} &= u_2 - v_b \rightarrow u_2 = v_b + u_{fb} \\ \underbrace{L_f \frac{di_{fc}}{dt} + R_f i_{fc}}_{u_{fc}} &= u_3 - v_c \rightarrow u_3 = v_c + u_{fc} \end{aligned} \quad (5)$$

where u_{fa} , u_{fb} and u_{fc} are the equivalent inputs.

From Fig.1, the capacitors currents are given by:

$$\begin{aligned} i_{ca} &= C_f \frac{dv_a}{dt} = i_{fa} - i_a \\ i_{cb} &= C_f \frac{dv_b}{dt} = i_{fb} - i_b \\ i_{cc} &= C_f \frac{dv_c}{dt} = i_{fc} - i_c \end{aligned} \quad (6)$$

The regulation of the load voltage using dynamic equation (6) with PI controller estimates the reference capacitor currents i_{ca}^* ; i_{cb}^* ; i_{cc}^* .

$$\begin{aligned} i_{ca}^* &= C_f \frac{dv_a}{dt} = i_{fa}^* - i_a \rightarrow i_{fa}^* = i_{ca}^* + i_a \\ i_{cb}^* &= C_f \frac{dv_b}{dt} = i_{fb}^* - i_b \rightarrow i_{fb}^* = i_{cb}^* + i_b \\ i_{cc}^* &= C_f \frac{dv_c}{dt} = i_{fc}^* - i_c \rightarrow i_{fc}^* = i_{cc}^* + i_c \end{aligned} \quad (7)$$

In order to reduce the output filter size and to reduce the losses caused by the damping resistor R_c , R_c is removed and the active damping control (ADC) is introduced.

IV. MATHEMATICAL MODEL OF ACTIVE DAMPING TECHNIQUE

Before demonstrating the effectiveness of ADC, the effect of the damping resistor R_c is analyzed.

A. Damping resistor model and transfer function of output filter

The conventional $L_f C_f$ output filter with damping resistor R_c is shown in Fig.5.

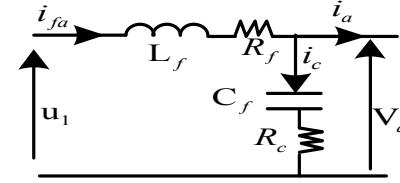


Fig. 5. Output filter with damping resistor R_c

The transfer function from Fig.5 is deduced as follow:

$$\frac{V_a}{U_1} = \frac{\frac{R_c}{jC_f\omega} + \frac{1}{jC_f\omega}}{\frac{R_c}{jC_f\omega} + jL_f\omega + R_f} = \frac{jR_c C_f \omega + 1}{j^2 L_f C_f \omega^2 + j\omega(R_c C_f + jR_f C_f) + 1} \quad (8)$$

Using Laplace parameter $s = j\omega$, the transfer function becomes:

$$G_0 = \frac{s R_c C_f + 1}{s^2 L_f C_f + s(R_c C_f + R_f C_f) + 1} \quad (9)$$

For the value of $L_f = 1.5e-3$ mH; $C_f = 20$ μ F; $R_f = 0.1$ Ω and for different values of damping resistor $R_c = [0 \ 5 \ 10]$ Ω ; the bode diagram of the transfer function G_0 is shown in Fig.6.

B. Power loss calculation in the damping Resistor R_c

The power losses for the damping resistor $R_c = 10 \Omega$ are calculated as follows:

$$Z_T = \sqrt{R_c^2 + \left(\frac{1}{C_f \omega}\right)^2} = \sqrt{100 + \left(\frac{1}{20 \cdot 10^{-6} \cdot 314}\right)^2} = 159.55 \Omega \quad (10)$$

$$I_c = \frac{V_{LL} / \sqrt{3}}{Z_T} = 1.37 A, \quad (11)$$

So the power losses in one phase are calculated as:

$$P_{Rc} = R_c \cdot I_c^2 = 10 \cdot (1.37)^2 = 18.77 W \quad (12)$$

The total power losses in three phases are deducted as:

$$P_{3\phi R_c} = 3 \cdot P_{Rc} = 3 \cdot 18.77 = 56.31 W \quad (13)$$

These losses are present 24 hours regardless of the loading condition. One remarks in Fig.6, the intersection point for different values of R_c gives the same band pass. It means there is no flexibility in the resonant frequency to help reducing the output filter size and reducing the power losses.

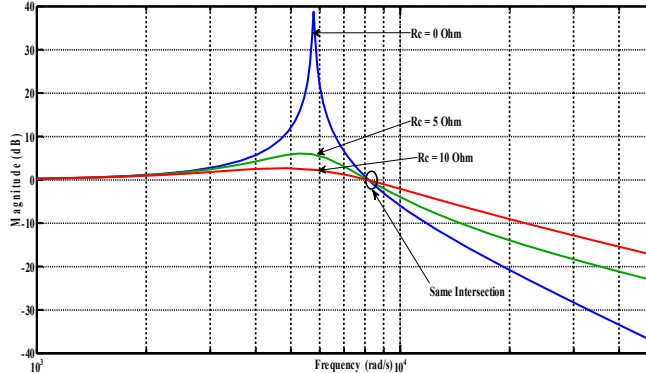


Fig. 6. Bode diagram of output filter with damping resistor R_c

C. Model of the active damping technique

Fig.7 shows the physical removal of damping resistor R_c . The objective is to develop a modeling approach to integrate the active damping technique in the control of the VSC but without any additional sensors and will be able to eliminate all losses caused by the damping resistor R_c . This approach improves the voltage quality at the PCC and increases the efficiency of the system. Fig.7 shows the new schema of $L_f C_f$ filter without damping resistor R_c .

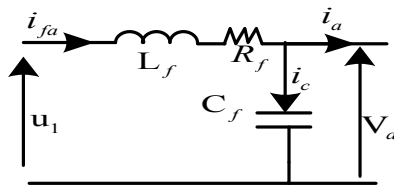


Fig. 7. Output filter with Active Damping technique

The theory of active damping is based on dynamical and current capacitor equations (5) and (6) of VSC.

Replacing equation (6) in (4), one obtains:

$$L_f \frac{d\left(C_f \frac{dv_a}{dt} + i_a\right)}{dt} + R_f \left(C_f \frac{dv_a}{dt} + i_a\right) = u_1 - v_a \quad (14)$$

Rearranging the eq.(14), one obtains

$$L_f C_f \frac{d^2 v_a}{dt^2} + R_f C_f \frac{dv_a}{dt} + v_a = u_1 - R_f i_a - L_f \frac{di_a}{dt} \quad (15)$$

The transfer functions of eq. (14), from v_a to u_1 is given by:

$$\left. \frac{v_a}{u_1} \right|_{ia=0} = \frac{1}{C_f L_f s^2 + R_f C_f s + 1} = \frac{1}{s^2 + \frac{R_f}{L_f} s + \frac{1}{C_f L_f}} \quad (16)$$

The resonant frequency of the $L_f C_f$ filter is defined as:

$$\omega_0 = \frac{1}{\sqrt{L_f C_f}} = \frac{1}{\sqrt{1.5 \cdot 10^{-3} \cdot 20 \cdot 10^{-6}}} = 5773.5 \text{ rad/s} \quad (17)$$

Let us define the eq.15 which gives the transfer function from u_1 to v_a by neglecting the current i_a and is considered as a perturbation [31].

$$L_f C_f \frac{d^2 v_a}{dt^2} + R_f C_f \frac{dv_a}{dt} + v_a = u_1 \quad (18)$$

Let's introduce the expression $k_c i_c$ in the right side of the dynamic eq.18, one obtains the following equation given by:

$$L_f C_f \frac{d^2 v_a}{dt^2} + R_f C_f \frac{dv_a}{dt} + v_a = u_1 - k_c i_c \quad (19)$$

Replacing $i_c = C_f \frac{dv_a}{dt} = C_f \cdot s \cdot v_a$ in (19), the new open loop transfer function $G_1(s)$ of the plant given by:

$$G_1(s) = \frac{v_a}{u_1} = \frac{1}{L_f C_f s^2 + (R_f + k_c) C_f s + 1} = \frac{1}{s^2 + \frac{(R_f + k_c)}{L_f} s + \frac{1}{L_f C_f}} \quad (20)$$

If one chooses the damping factor $\zeta = 0.7$ then the choice of k_c is calculated as follows:

$$2\zeta\omega_0 = \frac{(R_f + k_c)}{L_f} \quad (21)$$

$$k_c = 2\zeta\omega_0 L_f - R_f = 2 \cdot 0.7 \cdot 5773.5 \cdot 0.0015 - 0.1 = 12$$

In Fig.8, when the k_c increases, the damping is reduced as well as the band pass. This will help to increase the resonant frequency and to reduce the size of the output filter by choosing the appropriate value of k_c in order to increase the attenuation.

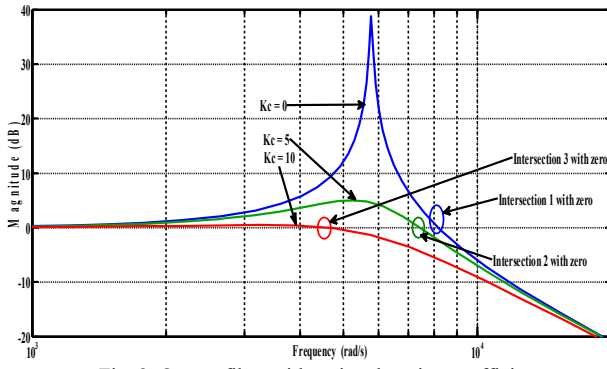


Fig. 8. Output filter with active damping coefficient

Fig.6, 8 and Fig.9 illustrate the comparison between the damping resistor R_c and active damping coefficient k_c . One notices during the variation of R_c [0 5 10] Ω , the intersection point remains the same (constant band pass), while with active damping k_c [0 5 10], the band pass is reduced. The active damping technique gives the flexibility to choose the optimal band pass to reduce the size of output filter $L_f C_f$ and to improve the voltage quality.

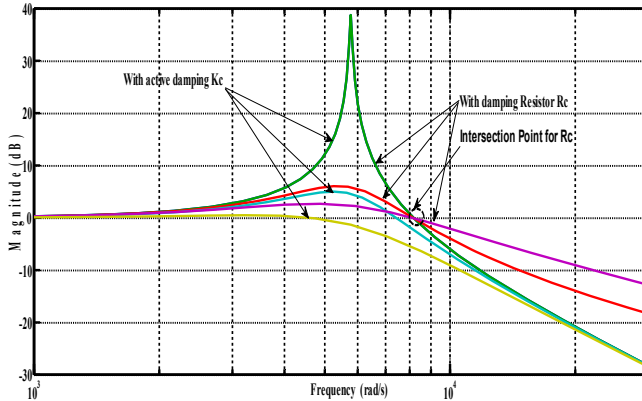


Fig. 9. Bode Diagram of R_c and k_c

D. Approach to reduce the value of output $L_f C_f$ using active damping technique

In order to reduce the size of the $L_f C_f$ filter, knowing that the inverter will compensate until the twenty fifth harmonics order as shown in Fig.10, let's say $25*60=1.5$ kHz. In Fig.11, the high harmonic frequency of the voltage inverter starts from 3.3 kHz, thereby, the resonant frequency is chosen at this value. One notices in Fig.8, the switching frequency of the inverter is 5 kHz.

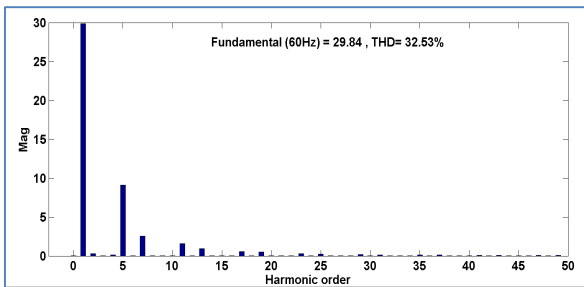


Fig. 10. Harmonic spectrum of load current

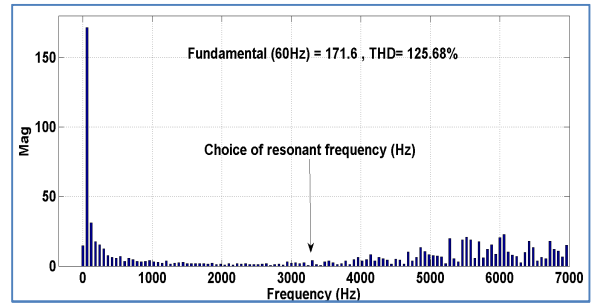


Fig. 11. Harmonic spectrum of inverter voltage

For fixed capacitor $C_{fl} = 7.5 \mu F$, the new value of L_{fl} is calculated as follows:

$$\omega_{01} = \frac{1}{\sqrt{L_{fl}C_{fl}}} \rightarrow L_{fl} = \frac{1}{(\omega_{01})^2 C_{fl}} = \frac{1}{(21000)^2 * 7.5 \cdot 10^{-6}} = 0.3 mH \quad (22)$$

With this new resonant frequency ω_{01} , the coefficient $k_{c1} = 8.7$ for the value of $\zeta = 0.7$. From Fig.12, this value of k_{c1} does not give complete satisfactory attenuation and filtering. For better attenuation and for good response one needs to increase the value of k_{c1} by decreasing the damping factor value to be $\zeta = 2.1$. The new value of k_{c1} is then calculated as follows:

$$k_{c1} = 2\zeta\omega_{01}L_{fl} - R_f = 2*2.1*21000*0.0003-0.1=26$$

In Fig.12, it is shown that the proposed approach technique based on active damping reduces the inductor value L_f by five times. The resonant frequency is shifted from ω_0 for value of $k_c = 20$ to ω_{01} for $k_{c1} = 26$. For both curves with $k_c = k_{c1} = 5$, one remarks that the phase margin is inside in its optimal value, this confirms the stability when shifting the resonant frequency. The value of $k_{c1}=26$ gives better attenuation and contribute to the voltage quality improvement. In order to prove the good choice of the new parameters of the output filter, the results of Pole-Zero Map are shown in Fig.13. For the new resonant frequency, three values of active damping coefficient k_{c1} are plotted in pole-zero maps. When k_{c1} increases, the pole of the transfer function of the filter starts initially with complex poles ($k_{c1}=5, k_{c1}=10$) and then for $k_{c1}=26$, the poles become real.

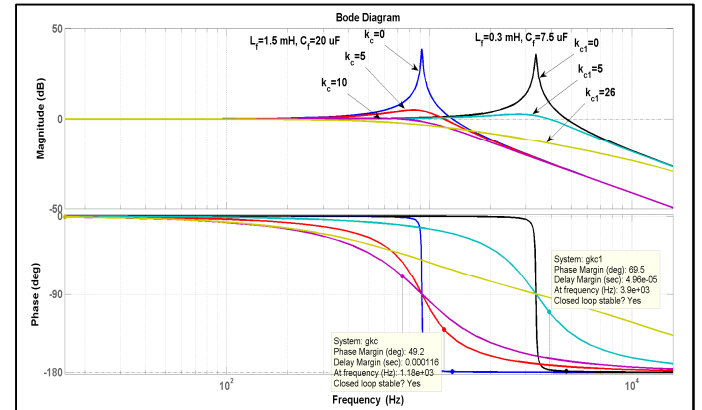


Fig. 12. New value of output filter $L_{fl} C_{fl}$ with new damping factor

This confirms that the shift of the resonant frequency from 0.92 kHz to 3.3 kHz does not affect the stability of the system, but allows reducing considerably the size of the LC filter.

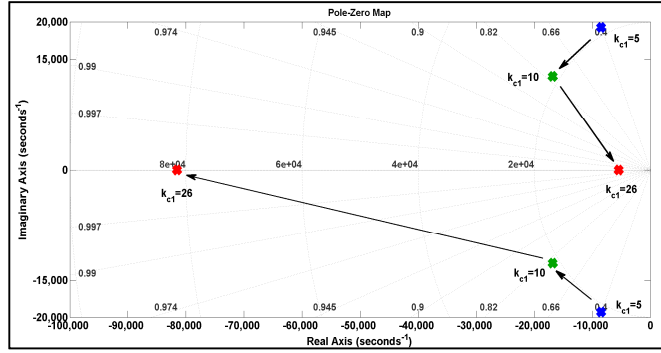


Fig. 13. Zero and pole maps for transfer functions of the output filter before and after value reduction

The new control approach of VSC including the proposed active damping technique is implemented in Fig.14:

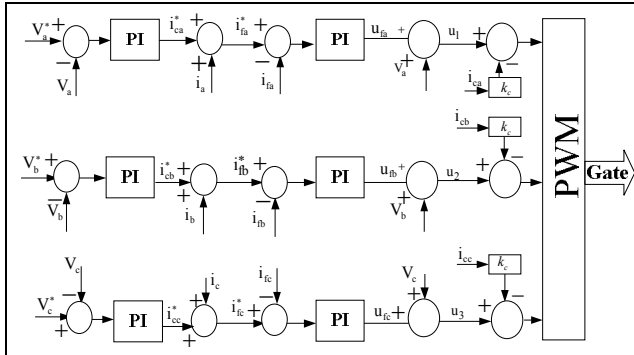


Fig. 14 Control of VSC inverter included active damping coefficient

V. FLS RULES AND BATTERY PROTECTION TECHNIQUE

A. Development of fuzzy logic rules

For a smart power management of the system, a fuzzy logic supervisor (FLS) is developed in order to control the power flow effectively, and to increase the global efficiency of the system. The objective is to build a smart control that takes into account the interaction between generation sources and a load demand, and regulates the SOC of batteries. The developed FSL was built on 25 fuzzy rules given in Table 1. Fig. 15 shows the FLS inputs variables $P_{reg} = P_{pv} - P_{pump} - P_L$, the state of charge of battery SOC (%) and the output variable P_{GGS} . The characteristic of GGS is used to extract the exact power needed by the load.

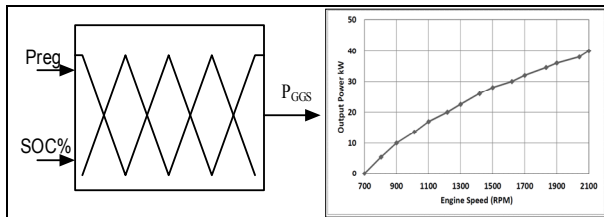


Fig. 15. FLS and typical variable spped of GGS [32]

Fig. 16, Fig17 and Fig.18 show the membership function of inputs and output variables.

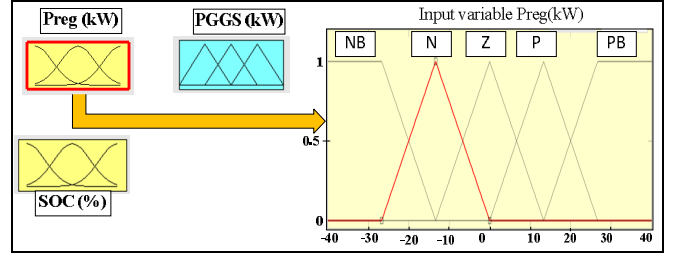


Fig.16. Membership function of input variable P_{reg}

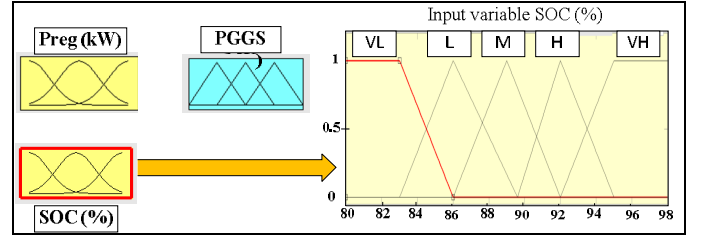


Fig. 17 Membership function of input variable SOC

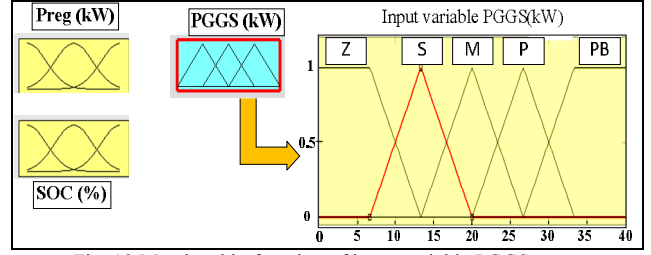


Fig. 18 Membership function of input variable PGGS

Table 1 resumes the 25 fuzzy logic rules developed for the power management of the system.

Table I: Fuzzy logic rules

	NB	N	Z	P	PB
VL	PB	PB	M	Z	Z
L	PB	PB	M	Z	Z
M	PB	M	Z	Z	Z
H	M	Z	Z	Z	Z
VH	M	M	Z	Z	Z

NB : Negative Big; N : Negative; Z : Zero; P : Positive; PB : Positive Big; VL:Very Low; L:Low; M:Medium; H:High; VH: Very High

The explanation of FLS rules following the instruction of the expert for the first line of table I is:

- If P_{reg} is NB and SOC is VL then P_{GGS} is PB, the gaz generator supplies entirely the full load.
- If P_{reg} is N and SOC is VL then P_{GGS} is PB, the gaz generator supplies the load power demand and also charges the battery

- If P_{reg} is Z and SOC is VL then PGGS is M, PV solar will supply alone all the load power and the battery will be charged by the PGGS
- If P_{reg} is P and SOC is VL then PGGS is Z, PV solar will supply the load demand and the difference is sent to the battery
- If P_{reg} is PB and SOC is VL then PGGS is Z, here the battery and the water pump will take additional power delivered by the PVA solar.

One deduces that if P_{reg} is negative then the power generated is not sufficient because the solar PVA is not delivering the required power. In this case a contribution of gas generator is essential to deliver the power difference. If it is positive, then extra power is delivered by the solar PVA, and in some cases, it may be used to charge the battery.

B. Battery overcharging protection and stability of the system

To protect the battery against overcharging and to avoid the extra power losses, a dc water pump is used as a dump load. As shown in Fig.1, the starting condition of the water pump is integrated in the control by comparing the measured battery voltage V_{Bat} and the maximum allowed battery voltage V_{Bat-Max}. If overvoltage or overcharging of the battery occurs, then the control signal is sent to the switch to activate the water pump. The pump will be deactivated when the battery voltage returns to the normal value. For the extra power not consumed by the load and in case of full battery charged the supervisor activates the dump load which is represented by the dc water pump or charging the electric vehicle. If during the night, the lack of solar irradiation and in case of empty battery energy capacity, the electric vehicle battery through the supervisor is solicited to supply the emergency load. The stability limit depends on the power balance controlled by the supervisor; if this limit is reached then the system should activate the security breaker to make off the PVA.

VI. SIMULATION AND EXPERIMENTAL RESULTS

A. Simulation results

Table II System parameters used in simulation

Load voltage frequency	60 Hz
Inductive filter (L _f)	1.5 mH
Inductive filter (L _{fl})	0.3 mH
Battery nominal voltage	500 V
Switching frequency	5 kHz
Rectifier nonlinear load (R _L and C _L)	10Ω, 1000 μF
DC capacitor (C _{dc})	5000 μF
PVA=40 kW, GGS = 40 kW	

Fig.16. shows the performance of the FLS to manage the power flow between the different energy sources. The power follows perfectly the rules of the FLS described in

the table1. The FLS provides the corresponding speed of GGS to deliver exactly the power to balance the system in case of insufficient solar power generation and may also charge the batteries. The FLS also controls the charging of batteries via SOC. If the SOC is more than 95%, then the extra power is sent to activate the water pump.

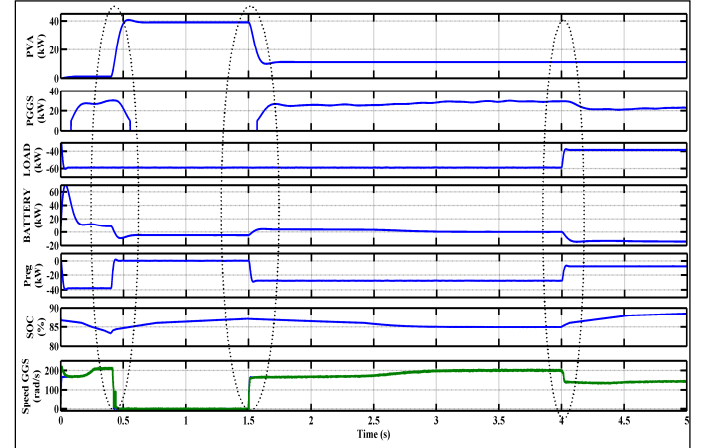


Fig. 19 Power flow and speed of the GGS

In Fig.19, during the transient start-up, the battery supplies alone the load power demand, the PVA is not contributing and the GGS is off. From t = 0.1 to 0.5s the GGS is switched ON and shares the power demand with the battery. From t = 0.5 to t = 1.5s, the PVA started delivering the power demand (40 kW), SOC of the battery remains constant and the GGS is then shutdown automatically. From t = 1.5 to t = 4s, the PVA generates only 10 kW, the GGS is then delivering the difference needed by the load (37 kW). From t = 4 to 5s, some loads are disconnected, but the PVA is still delivering only 10 kW, the GGS then generates 10 kW for the load and others 10 kW to charge the battery. During transient time, especially at start-up, the battery is supplying 100% the load, until the GGS reaches the nominal operation point and starts to feed fully the load instead of battery.

B. Experimental Result

Table III System parameters used in experimentation

Load voltage frequency	60 Hz
Inductive filter (L _f)	1.5 mH
Inductive filter (L _{fl})	0.3 mH
Battery nominal voltage	100 V
Switching frequency	5 kHz
Nonlinear load (R _L and C _L)	40Ω, 1000 μF
DC capacitor (C _{dc})	5000 μF

Fig. 20 shows the experimental setup in the laboratory and the system has been tested for different scenarios.

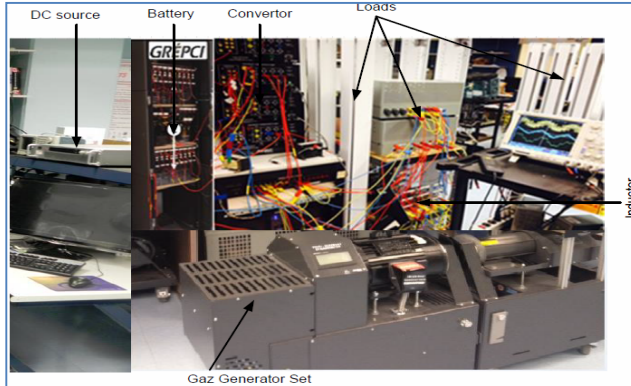


Fig. 20 Experimental Setup used for test

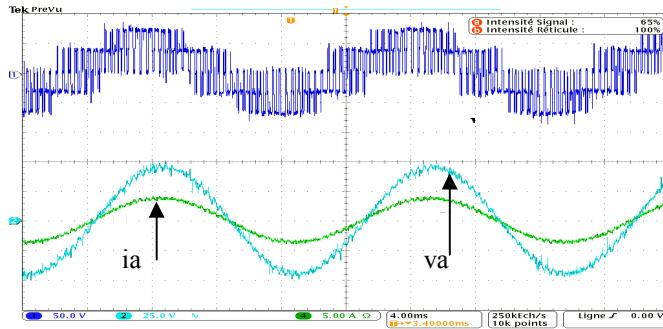


Fig. 21 Steady state response of the system

Fig. 21 shows the experimental results for steady state operation of the system with linear load. V_f , V_a and i_a representing the output voltage of VSC, the load voltage and the load current respectively. The good quality of the load voltage (THD = 3%) and in phase with the load current confirms the good performance of the output filter.

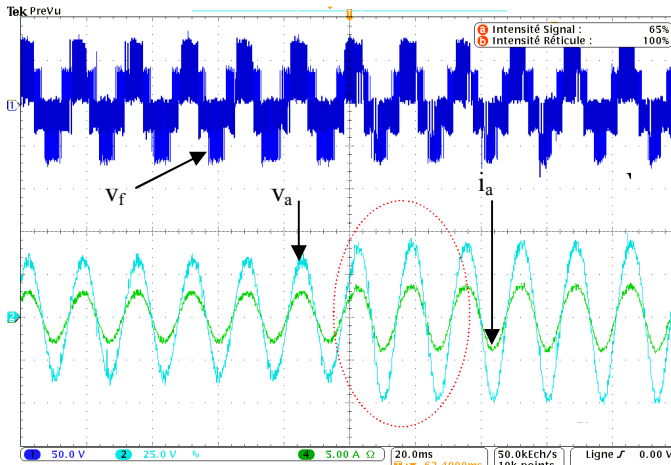


Fig. 22 Reference load voltage variation from 30 to 45 V

Fig. 22 shows the dynamic response of the system during the variation of the output reference voltage. The output voltage follows exactly the reference variation, satisfying the performance of the control algorithm. The dynamic response shows the fast response of the output voltage during the variation of the reference voltage.

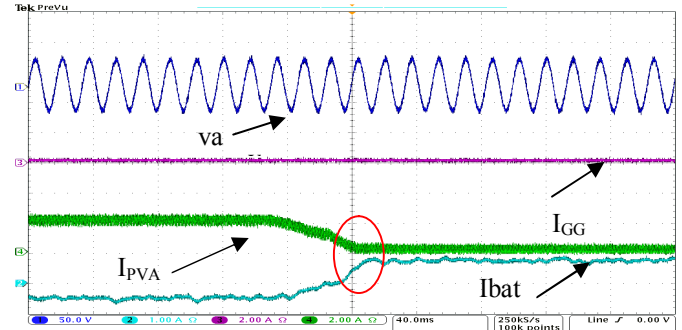


Fig. 23 Feeding of load from PVA and batteries

In Fig. 23, the system is tested for interaction between PVA, battery and GGS. At the beginning, the GGS is set to zero, the PVA generates more power than the load demand; the extra power is sent to charge the battery. When the PVA does not generate any power and GGS is still zero, the battery starts immediately sending power to satisfy the load demand. The battery is usually used to supply power for small applications such as lighting and TV at night.

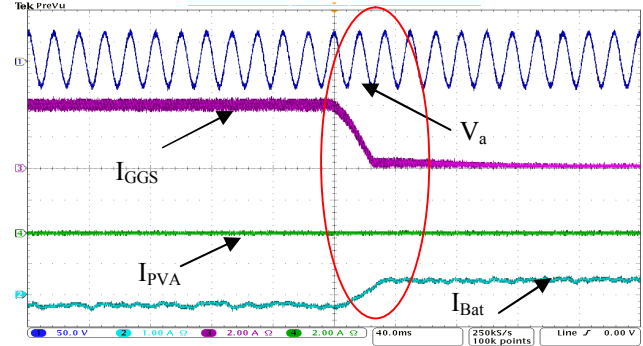


Fig. 24 Load voltage with GGS and batteries without PVA

Fig. 24 shows the dynamic response of system when I_{PVA} is zero, the GGS is turn on automatically to satisfy the load demand and also charges the battery. When the GGS is switched OFF, the battery will alone feed the load and the PVA is still OFF.

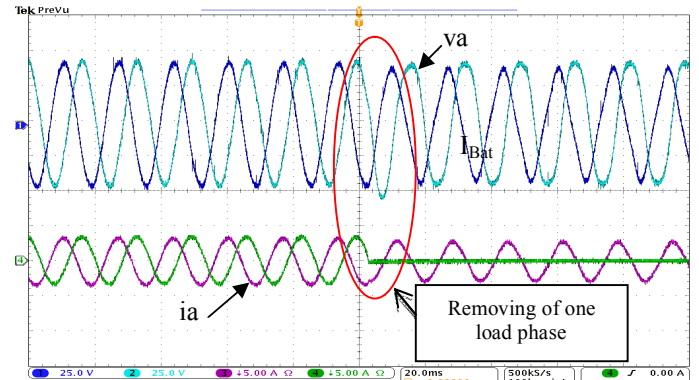


Fig. 25 Voltage regulation during connection and disconnection of one load phase current

Fig. 25 shows the perfect regulation of the voltage at the PCC during the removing of one phase load. This kind

of unpredictable change did not influence the functionality of the system due to the robustness of the control.

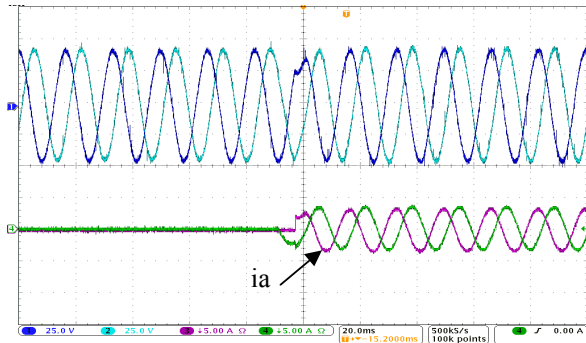


Fig.26 Voltage regulation during disconnection and connection

Fig.26 shows the same scenario as the fig. 25 but one phase load which was removed at the beginning was reconnected. The same performances of voltage regulation at the PCC are also seen.

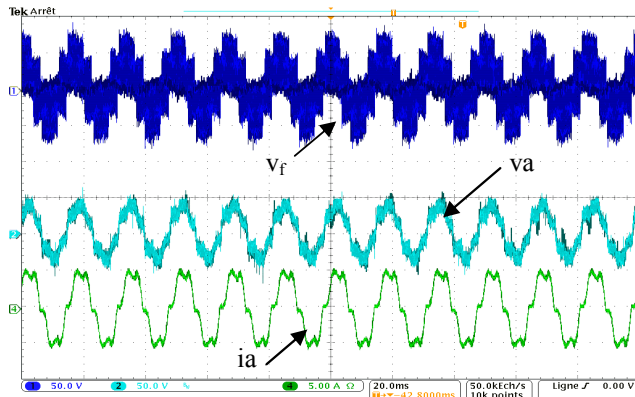


Fig.27 Experimental results without active damping

In Fig.27, the system is tested with nonlinear load and without active damping control. The load voltage is highly distorted, which means that the entire current harmonics are flowing through the capacitor of the output filter C_f which generates voltage harmonic.

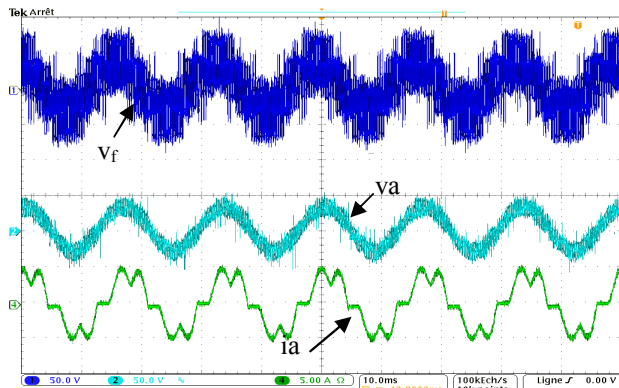


Fig.28 Experimental result including active damping

In Fig.28, the system is tested with nonlinear load including active damping control. The distortion of load voltage is significantly reduced, that means the current harmonics flows through the capacitor are much reduced, because the value of the capacitor C_f is reduced to C_{fl}

hence the impedance is increased which limits the current harmonics flowing through it.

VII. CONCLUSION

In this paper, three aspects have been studied for microgrid optimization. 1) A new approach of active damping control technique without using any additional current sensor has allowed reducing the losses in output filter and improved the voltage quality 2) The technique used to shift the resonant frequency to 21000 rad/s has permitted to reduce five times the size of LC filter while the stability of the system was not affected, 3) Finally, the fuzzy logic supervisor built on 25 rules has demonstrated its advantages by ensuring a smart power management of the system. The mixed operation of PVA and GGS has contributed in the battery size reduction while ensuring an uninterrupted power supply. The feasibility and effectiveness of this optimized microgrid system for remote area were evaluated with different simulation studies and have been validated experimentally in the laboratory setup.

REFERENCES

- [1] B. Zhao, X. Zhang, J. Chen, C. Wang and L. Guo, "Operation Optimization of Standalone Microgrids Considering Lifetime Characteristics of Battery Energy Storage System," *IEEE Trans. Sustainable Energy*, vol. 4, no. 4, pp. 934-943, Oct. 2013.
- [2] I. Y. Chung, W. Liu, D. A. Cartes, E. G. Collins, Jr., and S. I. Moon, "Control methods of inverter-interfaced distributed generators in a microgrid system," *IEEE Trans. Ind. Appl.*, vol. 46, no. 3, pp. 1078–1088, May/Jun. 2010.
- [3] I. P. Nikolakakos, I. A. Al-Zyoud, H. H. Zeineldin, M. S. El-Moursi and A. S. Al-Hinai, "Enhancement of islanded droop-controlled microgrid performance via power filter design," *PES General Meeting | Conf. & Exposition, 2014 IEEE*, National Harbor, MD, 2014, pp. 1-5.
- [4] M. Kumar, S. C. Srivastava and S. N. Singh, "Control Strategies of a DC Microgrid for Grid Connected and Islanded Operations," in *IEEE Tran. Smart Grid*, vol. 6, no. 4, pp. 1588-1601, July 2015.
- [5] S. A. Pourmousavi, M. H. Nehrir and R. K. Sharma, "Multi-Timescale Power Management for Islanded Microgrids Including Storage and Demand Response," in *IEEE Trans. Smart Grid*, vol. 6, no. 3, pp. 1185-1195, May 2015.
- [6] P. C. Loh, D. Li, Y. K. Chai and F. Blaabjerg, "Autonomous Control of Interlinking Converter With Energy Storage in Hybrid AC-DC Microgrid," in *IEEE Trans. Ind. Appl.*, vol. 49, no. 3, pp. 1374-1382, May-June 2013.
- [7] A. Banerji, S. K. Biswas and B. Singh, "Enhancing Quality of Power to Sensitive Loads With Microgrid," in *IEEE Trans. Ind. Appl.*, vol. 52, no. 1, pp. 360-368, Jan.-Feb. 2016.doi: 10.1109/TIA.2015.247884
- [8] A. Trentin, P. Zanchetta, P. W. Wheeler, and J. Clare, "Automated optimal design of input filters for direct ac/ac matrix converters," *IEEE Trans. Ind. Electron.*, vol. 59, no. 7, pp. 2811–2823, Jul. 2011.
- [9] F.S Tidjani, A. Hamadi, A. Chandra and P. Pillay, "Control strategy for improving the power flow between home integrated photovoltaic system, plug-in hybrid electric vehicle and distribution network," in *Proc. IEEE Ind. Electron. Conf.*, vol. , no. , pp.2003,2009, Oct. 29 2014-Nov. 1 2014.
- [10] R. N. Beres, X. Wang, F. Blaabjerg, M. Liserre and C. L. Bak, "Optimal Design of High-Order Passive-Damped Filters for Grid-Connected Applications," *IEEE Trans. on Power Electronics*, vol. 31, no. 3, pp. 2083-2098, March 2016.
- [11] D. Pan, X. Ruan,C.Bao,W. Li, andX.Wang, "Capacitor-current-feedback active damping with reduced computation delay for

- improving robustness of LCL-type grid-connected inverter,” *IEEE Trans. Power Electron.*, vol. 29, no. 7, pp. 3414–3427, Jul. 2014.
- [12] R. Pena-Alzola, M. Liserre, F. Blaabjerg, R. Sebastian, J. Dannehl, and F.W. Fuchs, “Systematic design of the lead-lag network method for active damping in LCL-filter based three phase converters,” *IEEE Trans. Ind. Inf.*, vol. 10, no. 1, pp. 43–52, Feb. 2014.
- [13] X. Li, X. Wu, Y. Geng, X. Yuan, C. Xia, and X. Zhang, “Wide damping region for LCL-type grid-connected inverter with an improved capacitorcurrent- feedback method,” *IEEE Trans. Power Electron.*, vol. 30, no. 9, pp. 5247–5259, Sep. 2015.
- [14] X. Wang, F. Blaabjerg, and P. C. Loh, “Virtual RC damping of LCLfiltered voltage source converters with extended selective harmonic compensation,” *IEEE Trans. Power Electron.*, vol. 30, no. 9, pp. 4726–4737, Sep. 2015.
- [15] N. L. Diaz, T. Dragičević, J. C. Vasquez and J. M. Guerrero, “Intelligent Distributed Generation and Storage Units for DC Microgrids—A New Concept on Cooperative Control Without Communications Beyond Droop Control,” *IEEE Trans. Smart Grid*, vol. 5, no. 5, pp. 2476–2485, Sept. 2014.
- [16] M. H. Moradi, M. Eskandari and S. Mahdi Hosseini, “Operational Strategy Optimization in an Optimal Sized Smart Microgrid,” *IEEE Trans. Smart Grid*, vol. 6, no. 3, pp. 1087–1095, May 2015.
- [17] Jinwei He, Yun Wei Li and F. Blaabjerg, “Flexible Microgrid Power Quality Enhancement Using Adaptive Hybrid Voltage and Current Controller,” in *IEEE Trans. Ind. Electron.*, vol. 61, no. 6, pp. 2784–2794, June 2014.
- [18] H. Kanchev, D. Lu, B. Francois and V. Lazarov, “Smart monitoring of a microgrid including gas turbines and a dispatched PV-based active generator for energy management and emissions reduction,” in *Proc. IEEE PES conf.*, vol. , no., pp.1,8, 11-13 Oct. 2010.
- [19] H. Fakham, P. Degobert and B. Francois, “Control system and power management for a PV based generation unit including batteries,” in *Proc. Electrical Machines and Power Electron Conf.*, vol. , no., pp.141,146, 10-12 Sept. 2007.
- [20] J. Andreu, I. Kortabarria, E. Ormaetxea, E. Ibarra, J. L. Martin, and S. Apinaniz, “A step forward towards the development of reliable matrix converters,” *IEEE Trans. Ind. Electron.*, vol. 59, no. 1, pp. 167–183, Jan. 2012.
- [21] X. Liu, P. C. Loh, P. Wang, F. Blaabjerg, Y. Tang, and E. A. Al-Ammar, “Distributed generation using indirect matrix converter in reverse power mode,” *IEEE Trans. Power Electron.*, vol. 28, no. 3, pp. 1072–1082, Mar.2013.
- [22] A. Trentin, P. Zanchetta, P.W. Wheeler, and J. Clare, “Automated optimal design of input filters for direct ac/ac matrix converters,” *IEEE Trans. Ind. Electron.*, vol. 59, no. 7, pp. 2811–2823, Jul. 2011.
- [23] M. Rivera, J. Rodriguez, B. Wu, J. Espinoza, and C. Rojas, “Current control for an indirect matrix converter with filter resonance mitigation,” *IEEE Trans. Ind. Electron.*, vol. 59, no. 1, pp. 71–79, Jan. 2012.
- [24] F.S Tidjani and A. Chandra, “Integration of renewable energy sources and the utility grid with the Net Zero Energy Building in Republic of Chad,” in *Proc. IEEE Ind. Electron.*, vol. , no., pp.1025,1030, 25-28 Oct. 2012
- [25] J. Pillai and B. Bak-Jensen, “Integration of vehicle-to-grid in the western Danish power system,” *IEEE Trans. Sustainable Energy*, vol. 2, no. 1, pp. 12–19, Jan. 2011.
- [26] S. Han, S. Han, and K. Sezaki, “Development of an optimal vehicle-to grid aggregator for frequency regulation,” *IEEE Trans. Smart Grid*, vol. 1, no. 1, pp. 65–72, Jun. 2010.
- [27] T. Lin and S. Tsumoto, “Qualitative fuzzy sets and granularity,” in *Proc. 7th IEEE Int. Conf. Cogn. Inf.*, 2008, pp. 435–440, ICCI 2008.
- [28] K. Wei, Z. Wang, and Q. Wang, “Describing fuzzy sets using a new concept: Fuzzify functor,” *Optoelectron. Lett.*, vol. 5, no. 1, pp. 69–72, 2009.
- [29] J. Garibaldi, M. Jaroszewski, and S. Musikaswan, “Nonstationary fuzzy sets,” *IEEE Trans. Fuzzy Syst.*, vol. 16, no. 4, pp. 1072–1086, 2008.
- [30] Tidjani, F.S.; Chandra, A.; Pillay, P., “Design of building integrated photovoltaic system to the grid with power quality improvement features for Central African countries,” in *Proc. IEEE Ind. Electron. conf.*, vol. , no., pp.2023,2029, Oct. 2014.

- [31] H. Y. Kanaan, C. Somers and K. Al-Haddad, “Design and implementation of a modified Sheppard-Taylor Power Factor Corrector operating in Discontinuous Capacitor Voltage Mode and very low output voltage level,” in *Proc. IEEE Ind. Electron conf.*, Vienna, 2013, pp. 7758–7762.
- [32] M. Rezkallah, A. Chandra and B. Singh, “Three-leg four-wire voltage source inverters for hybrid standalone system feeding unbalanced load,” in *Proc Ind. Electron.*, vol. , no., pp.1916,1921, 10-13 Nov. 2013.



Fadoula Souleyman Tidjani (SM'12) received the B. Tech. Degree and M.Tech degree in power electronics and Renewable Energy Management System from Russian St.Petersburg State Polytechnical University (SPbSPU), in 2006 and 2008 respectively. From 2010 to 2016, Fadoula is preparing his PhD in smart grid system at the École de Technologie Supérieure (ÉTS), Université du Québec, Montréal, QC, Canada, and He is also working in corporation as a developer of solar convertor, active harmonic filter and Energy management.



Abdelhamid Hamadi received the Bachelor of Engineering degree in power electronics from the University of Polytechnics, Ecole Nationale Polytechnique, Algiers, Algeria, in 1987, and the M.Sc. and Ph.D. degrees from the École de Technologie Supérieure, Montreal, QC, Canada, in 2004 and 2010, respectively, with theses entitled “Improved performance of the active filter: Application of the full proportional controller and fuzzy controller” and “Contribution to the study of hybrid power filters used to improve power quality in the electrical distribution network,” respectively. He is currently a Postdoctoral Fellow in the Department of Electrical Engineering, École de Technologie Supérieure. His research interests include the application of power electronics in distribution systems, power quality analysis, active power filters, hybrid power filters, series hybrid filters, passive filters, and renewable energy.



Ambrish Chandra (SM'99–F'14) received the Electrical engineering degree from Indian Institute of Technology (IIT), Roorkee, India, in 1977 the M.Tech. degree in power apparatus and systems from the IIT, in 1980, and the Ph.D. degree from the University of Calgary, Canada, in 1987. From 2012 to 2015, he was the Director of the graduate program on “renewable energy and energy efficiency” at the École de Technologie Supérieure (ÉTS), Université du Québec, Montréal, QC, Canada, where since 1994, he has been a Professor with the Department of Electrical Engineering. His research interests include power quality, active filters, static reactive power compensation, flexible ac transmission systems (FACTS), and control and integration of renewable energy resources. He has coauthored the book *Power Quality—Problems and Mitigation Techniques* (Wiley, 2015). He is a Distinguished Lecturer of IEEE Power and Energy Society and also of IEEE Industry Application Society. Dr. Chandra is an Associate Editor of the *IEEE Transactions on Industrial Electronics*. He is a Professional Engineer in the Province of Quebec, Canada.



Pragasen Pillay (F'05) received the Bachelor's degree and Master's degree in electrical engineering from the University of Kwa-Zulu Natal, Durban, South Africa, in 1981 and 1983, respectively, and the Ph.D. degree in electrical engineering from Virginia Polytechnic Institute and State University, Blacksburg, VA, USA, in 1987.

He is currently a Professor in the Department of Electrical and Computer Engineering, Concordia University, Montréal, Québec, Canada, where he is currently the Natural Sciences and Engineering Research Council of Canada (NSERC), Ottawa, ON, Canada/ Hydro-Québec Industrial Research Chair, Montréal, Québec, Canada.



Auguste Ndoungou received the Ph.D. degree from the University of Paris XI, France, in 1996. From 1997, he has been a Professor with the Electrical Engineering, École Polytechnique de Masuku, Gabon. He is currently an invited professor in the department of electrical engineering, École de Technologie Supérieure, Montreal, Canada. His research interests include power electronics, power quality, and renewable energy.